The Astrophysical Journal Letters, 955:L4 (8pp), 2023 September 20 https://doi.org/10.3847/2041-8213/ace112

Coronal Heating Rate in the Slow Solar Wind

Daniele Telloni[1], Marco Romoli[2], Marco Velli[3], Gary P. Zank[4,5], Laxman Adhikari[4], Cooper Downs[6], Aleksandr Burtovoi[7], Roberto Susino[1], Daniele Spadaro[8], Lingling Zhao[4], Alessandro Liberatore[9], Chen Shi[3], Yara De Leo[10,11], Lucia Abbo[1], Federica Frassati[1], Giovanna Jerse[12], Federico Landini[1], Gianalfredo Nicolini[1], Maurizio Pancrazzi[1], Giuliana Russano[13], Clementina Sasso[13], Vincenzo Andretta[13], Vania Da Deppo[14], Silvano Fineschi[1], Catia Grimani[15,16], Petr Heinzel[17,18], John D. Moses[19], Giampiero Naletto[20], Marco Stangalini[21], Luca Teriaca[10], Michela Uslenghi[22], Arkadiusz Berlicki[18,23], Roberto Bruno[24], Gerardo Capobianco[1], Giuseppe E. Capuano[8,11], Chiara Casini[14,25], Marta Casti[26], Paolo Chioetto[14,25], Alain J. Corso[14], Raffaella D'Amicis[24], Michele Fabi[15,16], Fabio Frassetto[14], Marina Giarrusso[2], Silvio Giordano[1], Salvo L. Guglielmino[8], Enrico Magli[27], Giuseppe Massone[1], Mauro Messerotti[12,28], Giuseppe Nisticò[29], Maria G. Pelizzo[30], Fabio Reale[31,32], Paolo Romano[8], Udo Schühle[10], Sami K. Solanki[10], Thomas Straus[13], Rita Ventura[8], Cosimo A. Volpicelli[1], Luca Zangrilli[1], Gaetano Zimbardo[29], Paola Zuppella[14], Stuart D. Bale[33,34], and Justin C. Kasper[35,36]

[1] National Institute for Astrophysics, Astrophysical Observatory of Torino, Via Osservatorio 20, I-10025 Pino Torinese, Italy; daniele.telloni@inaf.it
[2] University of Florence, Department of Physics and Astronomy, Via Giovanni Sansone 1, I-50019 Sesto Fiorentino, Italy
[3] Earth, Planetary, and Space Sciences, University of California, Los Angeles, CA 90095, USA
[4] Center for Space Plasma and Aeronomic Research, University of Alabama in Huntsville, Huntsville, AL 35805, USA
[5] Department of Space Science, University of Alabama in Huntsville, Huntsville, AL 35805, USA
[6] Predictive Science Inc., San Diego, CA 92121, USA
[7] National Institute for Astrophysics, Astrophysical Observatory of Arcetri, Largo Enrico Fermi 5, I-50125 Firenze, Italy
[8] National Institute for Astrophysics, Astrophysical Observatory of Catania, Via Santa Sofia 78, I-95123 Catania, Italy
[9] Jet Propulsion Laboratory, California Institute of Technology, Pasadena, CA 91109, USA
[10] Max Planck Institute for Solar System Research, Justus-von-Liebig-Weg 3, D-37077 Göttingen, Germany
[11] University of Catania, Department of Physics and Astronomy, Via Santa Sofia 64, I-95123 Catania, Italy
[12] National Institute for Astrophysics, Astronomical Observatory of Trieste, Località Basovizza 302, I-34149 Trieste, Italy
[13] National Institute for Astrophysics, Astronomical Observatory of Capodimonte, Salita Moiariello 16, I-80131 Napoli, Italy
[14] National Research Council, Institute for Photonics and Nanotechnologies, Via Trasea 7, I-35131 Padova, Italy
[15] University of Urbino Carlo Bo, Department of Pure and Applied Sciences, Via Santa Chiara 27, I-61029 Urbino, Italy
[16] National Institute for Nuclear Physics, Section in Florence, Via Bruno Rossi 1, I-50019 Sesto Fiorentino, Italy
[17] Czech Academy of Sciences, Astronomical Institute, Fričova 298, CZ-25165 Ondřejov,Ondřejov, Czechia
[18] University of Wrocław, Centre of Scientific Excellence—Solar and Stellar Activity, ul. Kopernika 11, PL-51-622 Wrocław, Poland
[19] National Aeronautics and Space Administration, Headquarters, Washington, DC 20546, USA
[20] University of Padua, Department of Physics and Astronomy, Via Francesco Marzolo 8, I-35131 Padova, Italy
[21] Italian Space Agency, Via del Politecnico snc, I-00133 Roma, Italy
[22] National Institute for Astrophysics, Institute of Space Astrophysics and Cosmic Physics of Milan, Via Alfonso Corti 12, I-20133 Milano, Italy
[23] University of Wrocław, Astronomical Institute, Kopernika 11, PL-51622 Wrocław, Poland
[24] National Institute for Astrophysics, Institute for Space Astrophysics and Planetology, Via del Fosso del Cavaliere 100, I-00133 Roma, Italy
[25] Centre of Studies and Activities for Space "Giuseppe Colombo", Via Venezia 15, I-35131 Padova, Italy
[26] The Catholic University of America at the National Aeronautics and Space Administration, Goddard Space Flight Center, Greenbelt, MD 20771, USA
[27] Politecnico of Turin, Department of Electronics and Telecommunications, Corso Duca degli Abruzzi 24, I-10129 Torino, Italy
[28] University of Trieste, Department of Physics, Via Alfonso Valerio 2, I-34127 Trieste, Italy
[29] University of Calabria, Department of Physics, Ponte Pietro Bucci Cubo 31C, I-87036 Rende, Italy
[30] University of Padua, Department of Information Engineering, Via Giovanni Gradenigo 6, I-35131 Padova, Italy
[31] University of Palermo, Department of Physics and Chemistry - Emilio Segrè, Piazza del Parlamento 1, I-90134 Palermo, Italy
[32] National Institute for Astrophysics, Astronomical Observatory of Palermo, Piazza del Parlamento 1, I-90134 Palermo, Italy
[33] Space Sciences Laboratory, University of California, Berkeley, CA 94720, USA
[34] Physics Department, University of California, Berkeley, CA 94720, USA
[35] BWX Technologies, Inc., Washington, DC 20002, USA
[36] Climate and Space Sciences and Engineering, University of Michigan, Ann Arbor, MI 48109, USA
Received 2023 May 8; revised 2023 June 7; accepted 2023 June 21; published 2023 September 14

Abstract

This Letter reports the first observational estimate of the heating rate in the slowly expanding solar corona. The analysis exploits the simultaneous remote and local observations of the same coronal plasma volume, with the Solar Orbiter/Metis and the Parker Solar Probe instruments, respectively, and relies on the basic solar wind magnetohydrodynamic equations. As expected, energy losses are a minor fraction of the solar wind energy flux, since most of the energy dissipation that feeds the heating and acceleration of the coronal flow occurs much closer to the Sun than the heights probed in the present study, which range from 6.3 to 13.3 $R_{\odot}$. The energy deposited to the supersonic wind is then used to explain the observed slight residual wind acceleration and to maintain the plasma in a nonadiabatic state. As derived in the Wentzel–Kramers–Brillouin limit, the present energy transfer rate

estimates provide a lower limit, which can be very useful in refining the turbulence-based modeling of coronal heating and subsequent solar wind acceleration.

Unified Astronomy Thesaurus concepts: Magnetohydrodynamics (1964); Magnetohydrodynamical simulations (1966); Interplanetary turbulence (830); Solar corona (1483); Solar coronal heating (1989); Solar wind (1534); Solar physics (1476); The Sun (1693)

1. Introduction

Central to the heating and subsequent acceleration of the coronal plasma is the identification of the physical mechanisms responsible for transporting the energy available in the photospheric motions to the corona, where it is dissipated by raising the temperature to a million degrees, sufficient for the plasma to overcome the Sun's gravity and thus expand into the heliosphere, forming the solar wind (Parker 1958). It is worth noting that this thermal driving can only account for the acceleration of the slowest coronal flows, while for the higher-speed streams to be accelerated, an additional source of energy is required, whose dissipation results in further heating and thus transition to a faster wind regime. The nonresonant dissipation of low-frequency magnetohydrodynamic (MHD) turbulent fluctuations is to date the most widely accepted heating mechanism, whether for fast or slow wind.

However, a key element for any heating model—namely, an estimate of the coronal energy transfer rate and its radial dependence—is still missing. This is basically because coronal measurements of the magnetic field and nonthermal plasma motions (related to turbulence), i.e., the Alfvén wave energy, are lacking (or at best inconclusive). In some fluid models (e.g., Holzer & Axford 1970; McKenzie et al. 1995), an ad hoc heating function, which decays exponentially with height over a prescribed dissipation length scale, is assumed to account for the energy deposition per unit volume. Other approaches resort to the use of numerical simulations in order to derive the coronal heating rate profile (e.g., Dmitruk et al. 2002).

Local single-point measurements of the turbulent energy cascade rate, which is directly related to the solar wind heating rate, are widely available at various heliospheric heights. Although a detailed discussion of turbulent heating rate estimates in the solar wind is beyond the scope of this article (the interested reader is referred to the comprehensive review by Marino & Sorriso-Valvo 2023), the following works are worth mentioning. Sorriso-Valvo et al. (2007) first applied the generalized form of the Yaglom law for MHD turbulence (as derived by Politano & Pouquet 1998) to Ulysses data (Wenzel et al. 1992) to derive the energy flux of the turbulent cascade in high-speed solar streams sampled at 3–4 au. Zhao et al. (2022) extended this approach to the first sub-Alfvénic interval observed with the Parker Solar Probe (PSP; Fox et al. 2016) at 0.09 au, using both incompressible and compressible formalisms for the equivalent Yaglom law (Andrés et al. 2019) and finding a higher average energy cascade rate than in the surrounding super-Alfvénic regions. Adopting the turbulence cascade model developed by Tu (1988) and exploiting PSP measurements, Wu et al. (2020) derived a formula for relating the radial scaling of the low-frequency spectral break to the energy supply rate in the slow solar wind, from 0.17 to 0.7 au. These authors found that at distances greater than 0.25 au from the Sun, injected and dissipated energies are of the same order, suggesting that the slow solar wind expands almost adiabatically. Deriving straightforward expressions for the turbulent heating rate, Adhikari et al. (2022) reported, from both observational and theoretical perspectives, on the radial evolution of the energy dissipation rate from 0.17 to 0.83 au, using PSP and Solar Orbiter (SO; Müller et al. 2020) data. It is true that some authors have exploited remote observations of the solar corona to probe the turbulent properties of coronal flows and thus derive constraints or upper limits on the rate of energy deposition in the corona (Chandran et al. 2009; Cranmer 2020; Sasikumar Raja et al. 2021). Yet, all these studies make extensive use of unknown parameter assumptions and are either highly model-dependent or based on numerical simulations. Although extremely important, these works do not provide direct, empirical observations of the coronal heating rate, as in the present study.

Quadratures between two spacecraft have already proved useful in linking local turbulent properties with the fluid parameters of remotely observed coronal flows (Telloni et al. 2021a, 2022a). However, the special orbital configuration between the PSP and SO spacecraft that occurred on 2022 June 1 offers an almost unique opportunity. Indeed, during this quadrature, PSP entered the portion of the plane of the sky (POS) imaged by the Metis coronagraph (Antonucci et al. 2020; Fineschi et al. 2020) on board SO. As described in the following, this allows the first ever observational estimate of the energy deposition rate in the solar corona, from 6.3 to 13.3 $R_\odot$, without having to invoke any model or ad hoc parameter assumptions. Indeed, the simultaneous remote and in situ measurements of the same coronal flow, associated with solving the basic equations for a steady-state, radial plasma flow, allow an empirical low-speed solar wind model to be derived. In addition, in the Wentzel–Kramers–Brillouin (WKB) theory approximation, the energy of the outward Alfvén wave flux and, in turn, the energy transfer rate, can be extended from the PSP location to the whole range of coronal heights observed with Metis. This is the aim of the present Letter, whose plan is as follows: Metis/PSP data and equation description (Section 2), then derivation of the empirical wind and turbulent model along with relevant discussion (Section 3).

2. SO/Metis–PSP Data and MHD Equations

On 2022 June 1, at 22:40 UT, when SO was at 0.936 au, PSP was in quadrature while orbiting at 13.3 $R_\odot$. An SO spacecraft roll of 45° along with an off-pointing of 1 $R_\odot$ toward the west limb was performed for PSP to squeeze into the Metis POS, which extended from about 6.3–13.3 $R_\odot$. Metis observations are supported by a 3D MHD modeling of the solar corona developed by Predictive Science Incorporated (PSI; Mikić et al. 2018). This is based on photospheric magnetic field measurements acquired by the Helioseismic and Magnetic Imager (Scherrer et al. 2012) on board the Solar Dynamics Observatory (Pesnell et al. 2012) and driven by a heating mechanism fed by the dissipation of low-frequency Alfvén waves.

Figure 1(a) shows the visible light observations of the coronal polarized Brightness (pB) obtained with Metis during the quadrature with PSP, marked with a blue dot and calibrated according to De Leo et al. (2023). PSP, 3.°6 below the

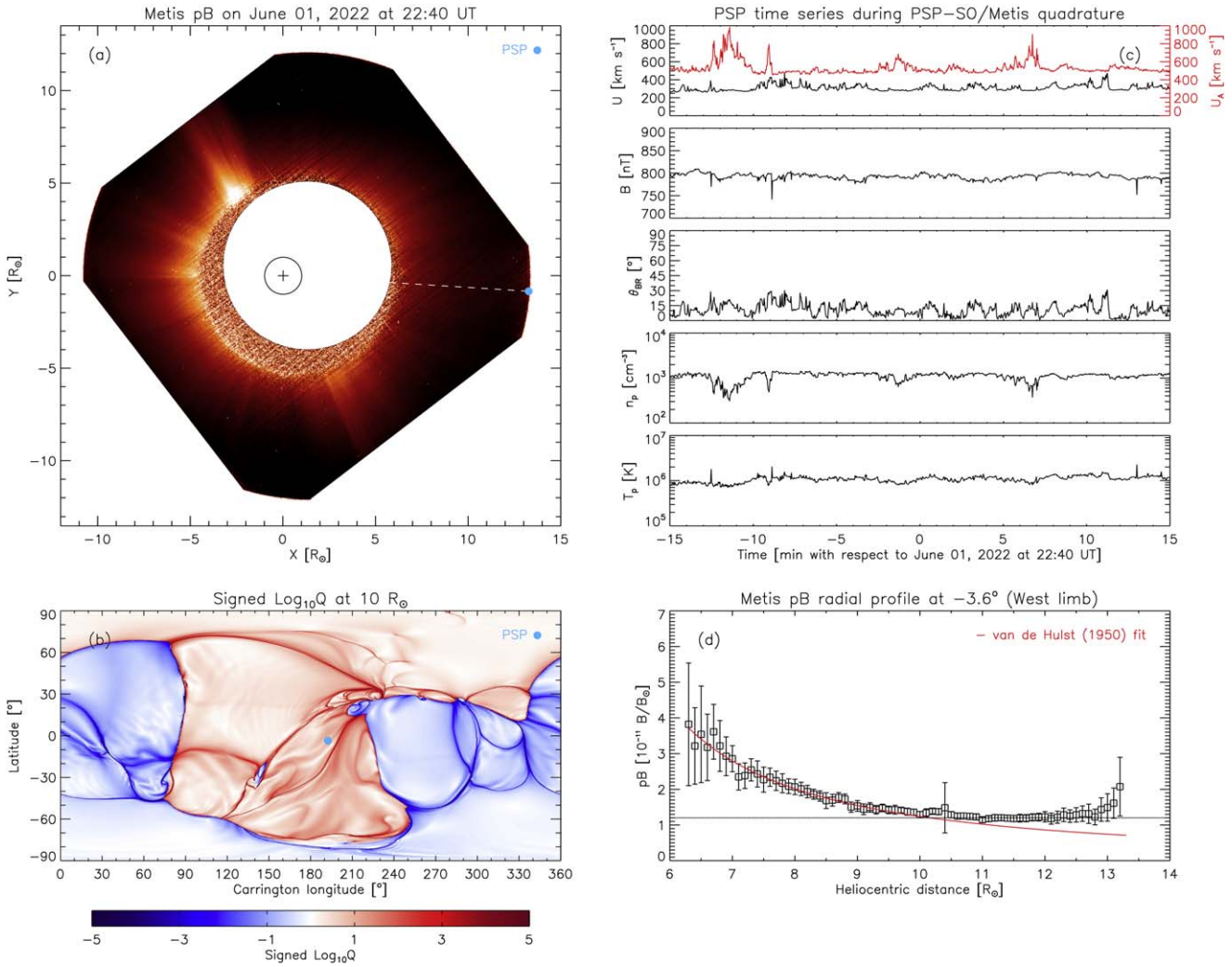

Figure 1. (a) Metis pB image on 2022 June 1 at 22:40 UT with PSP marked in its POS as a blue dot; the PSP direction is indicated by a white dashed line. (b) Projection of the PSP position (blue dot) onto the Carrington map of the squashing factor Q at 10 $R_\odot$. (c) PSP magnetic field and plasma time series (from top to bottom: wind bulk and Alfvén speed, magnetic field intensity and angle with the radial, and proton density and temperature) during the quadrature with SO. (d) Radial profile of the Metis pB observations at the latitude corresponding to the PSP location (open squares), along with the van de Hulst (1950) power-law fit (red line); the horizontal line at 1.2×10^{-11} $B/B_\odot$ represents the flattening level, probably due to the contamination by the F-corona and instrumental effects.

equatorial plane, was immersed in a diffuse coronal region devoid of emission-enhanced (i.e., denser) structures. Indeed, Figure 1(b), which displays the Carrington map of the squashing factor Q (Titov et al. 2011) at 10 $R_\odot$, clearly discloses that PSP sampled a low-latitude equatorial coronal hole, which, in this case, is near the outer positive polarity of a decaying active region from the previous rotation. Due to the pseudostreamer lobes bracketing the open flux (Figure 1(b)), however, the solar wind flow impinging on PSP was slow (Wang 1994), as shown in the top panel of Figure 1(c), which displays overall PSP plasma and magnetic field measurements acquired on a 0.5 hr long interval around the quadrature with SO/Metis (corresponding to $\pm 0.76°$ longitude with respect to the Metis POS). Specifically, from top to bottom, the panel presents the solar wind and Alfvén speed, the magnetic field vector strength and inclination with respect to the radial direction, and the proton density and temperature. This is a case of highly field-aligned ($\theta_{\rm BR} \sim 11°$) and sub-Alfvénic slow ($U \sim 310$ km s$^{-1} < U_A$) solar wind, which is additionally quite homogenous and stationary.

Finally, Figure 1(d) shows the pB radial profile at the latitude in the PSP direction (indicated by a white dashed line in Figure 1(a)). Relying on the approach initially advanced by van de Hulst (1950) and largely used with Metis observations (e.g., Romoli et al. 2021; Antonucci et al. 2023), the coronal electron density can be determined by inverting the coefficients of a power-law fit performed on the observed pB values. The combined effect of the contamination of the K-corona by the F-corona for distances larger than 10 $R_\odot$ (e.g., Howard et al. 2019) and a possible instrumental contribution appearing as a rise in pB values at the outer edge of the detector field of view (FOV) can in principle be responsible for the flattening of the pB radial profile at heights above 10 $R_\odot$ (around the value indicated by the horizontal line). Accordingly, the power-law fitting has been performed up to heights of 10 $R_\odot$ and then extrapolated beyond that (the red line in Figure 1(d)). Anticipating the results presented in the next section, it is already worth mentioning here that the electron density profile thus derived was checked and validated with the different technique from Hayes et al. (2001) and was verified to scale

approximately as r^{-2} at large distances from the Sun, at the outer edge of the Metis FOV (i.e., $r > 10\ R_\odot$).

In order to derive an empirical coronal flow model from the joint SO/Metis–PSP observations of the solar corona, the basic equations of solar wind theory need to be solved. A steady, radial flow of an ideal plasma is fully described by the equations for mass, momentum, and energy conservation below:

$$\frac{d}{dr}(\rho U A) = 0; \tag{1}$$

$$\rho U \frac{dU}{dr} = -\frac{dp}{dr} - \rho \frac{GM_\odot}{r^2}; \tag{2}$$

$$U \frac{dp}{dr} = -\gamma p \nabla \cdot \boldsymbol{U} + (\gamma - 1)\rho\epsilon, \tag{3}$$

where ρ is the mass density, $\boldsymbol{U}$ is the solar wind velocity, $A = f(r)r^2$ is the cross-sectional area of the flow tube connecting the equatorial coronal hole to the heliosphere (with $f(r)$ being the expansion factor), $p = nk_BT$ is the thermal pressure (with n, T, and k_B being the number density, temperature, and Boltzmann constant, respectively), G is the gravitational constant, $M_\odot$ is the solar mass, γ is the adiabatic index, ϵ is the heating per unit mass, and r is the radial coordinate. Note that the empirical model assumes only a very hot thermal plasma at the origin and that no distributed heating occurs due to the dissipation of turbulence. The heating rate ϵ is primarily due to low-frequency nearly incompressible turbulence and expressed as (Matthaeus et al. 1999a)

$$\epsilon \equiv \frac{1}{2}\alpha \frac{\langle |z^+|^2\rangle^2 \langle |z^-|^2\rangle + \langle |z^+|^2\rangle \langle |z^-|^2\rangle^2}{\lambda}, \tag{4}$$

where α is the Kármán-Taylor constant (usually around 0.125; see Usmanov et al. 2014, and references therein), $(1/2)\langle |z^\pm|^2\rangle$ are the energies associated with the outward/inward fluctuations given in terms of Elsässer variables, $\boldsymbol{z}^\pm = \boldsymbol{u} \pm \frac{\boldsymbol{b}}{\sqrt{\mu\rho}}$ (with $\boldsymbol{u}$ and $\boldsymbol{b}$ being the velocity and magnetic field fluctuations around the corresponding mean fields, $\langle \boldsymbol{U} \rangle$ and $\langle \boldsymbol{B} \rangle$, respectively, and μ the magnetic permeability), λ is the turbulence correlation length, and $\langle ... \rangle$ indicates time averaging over the data sample. Assuming that most of the turbulent energy comes from Alfvénic fluctuations, the system will be characterized by a balance between kinetic and magnetic energies, i.e., $\langle |\boldsymbol{u}|^2 \rangle \sim \langle |\boldsymbol{b}|^2 \rangle$. Equation (4) can thus be conveniently rewritten as (Adhikari et al. 2017)

$$\epsilon = \frac{E_b^{3/2}}{\left[C_k \log\left(\frac{1}{k_{inj}\lambda_b}\right)\right]^{3/2} \lambda_b}, \tag{5}$$

where $E_b = \langle |\boldsymbol{b}|^2 \rangle / (\mu\rho)$ and λ_b are the energy and correlation length associated with magnetic field fluctuations, respectively, $C_k = 1.6$ is the Kolmogorov constant, and $k_{inj} = 1.07 \times 10^{-9}$ km^{-1} is the large-scale injection wavenumber corresponding to the solar rotation frequency (related to each other by the Sun's rotational velocity). Equation (5) is derived on the basis of a dimensional analysis of the power spectral density of the turbulent magnetic energy E_b, assuming that it scales with the wavenumber k as Ak^{-1} and $C_k\epsilon^{2/3}k^{-5/3}$ (with A being a constant) in the energy-containing and inertial ranges, respectively, imposing equality of the spectrum branches at the frequency break k_b and integrating from k_{inj} to k_b. The only assumptions underlying the expression in Equation (5) are thus a Kolmogorov-like (Kolmogorov 1941) power law at fluid scales and that the correlation length λ_b corresponds to the spectral break k_b separating the injection and inertial ranges. Although customarily used (e.g., Telloni et al. 2022b), it is worth noting that it is a rough estimate of the heating rate that does not take into account, for example, the anisotropy in the solar wind turbulence fluctuations. In addition, in the Iroshnikov–Kraichnan picture of turbulence (Iroshnikov 1963; Kraichnan 1965), with a shallower spectrum scaling as $k^{-3/2}$ as usually observed closer to the Sun (e.g., Chen et al. 2020; Duan et al. 2020; Telloni et al. 2021b), the value for ϵ as provided by Equation (5) would be a factor of $\lambda_b^{-1/4}$ larger. Completing Equations (1)–(3) is the conservation of magnetic flux, $\frac{d}{dr}(BA) = 0$.

Integrating the equations for mass and magnetic flux conservation, it follows that the large-scale trends of the solar wind parameters (i.e., U, ρ, and B) can be estimated based on the values at some reference point $r = r_0$. Specifically, from (i) the estimates of the coronal mass density $\rho(r) = 0.95 m_p n_e$ (for a fully ionized plasma with 2.5% helium—Moses et al. 2020; and where m_p is the proton mass) as a function of the heliocentric distance derived from the pB Metis observations, (ii) the PSP plasma and magnetic field measurements at $r_0 = 13.3\ R_\odot$, and (iii) the expansion factor $f(r)$ provided by the PSI 3D MHD simulations (which results in only a weak dependence on height, i.e., $f(r) \sim 1$, away from the strong fields at the base of the corona, due to the rooting of the open flux near a low-lying pseudostreamer-type configuration), it is possible to empirically evaluate the solar wind speed and magnetic field strength radial profiles, $U(r)$ and $B(r)$, from 6.3 to 13.3 $R_\odot$. The Alfvén speed $U_A(r)$ and the solar wind energy flux $F_w(r)$ can then be immediately quantified in the Metis FOV as $U_A = B/\sqrt{\mu\rho}$ and $F_w = \frac{1}{2}\rho U^3$. In other words, in this joint SO/Metis–PSP analysis, Metis provides the radial trends for all the magnetofluid and turbulence parameters, while PSP, which definitely entered the corona (indeed, the Alfvén mach number $M_A = U/U_A \sim 0.59$), sets the (absolute) value at r_0.

The energy of the magnetic field fluctuations E_b and, in turn, the turbulent cascade (heating) rate ϵ can be empirically estimated deeper in the solar corona at the heights observed with Metis, by propagating the measurements made locally by PSP back to the Metis FOV. For simplicity, it is assumed the propagation equation for Alfvén waves in an expanding flow (Velli 1993), generalized to include a dissipation term $\mathcal{D}(\langle |z^+|^2\rangle^2 \langle |z^-|^2\rangle, \langle |z^+|^2\rangle \langle |z^-|^2\rangle^2, \lambda)$ and possible in situ sources of turbulence $\mathcal{S}$ (Zhou & Matthaeus 1990; Zank et al. 1996; Wang et al. 2022):

$$\frac{\partial \boldsymbol{z}^\pm}{\partial t} + (\boldsymbol{U} \pm \boldsymbol{U}_A) \cdot \nabla \boldsymbol{z}^\pm + \boldsymbol{z}^\mp \cdot \nabla(\boldsymbol{U} \mp \boldsymbol{U}_A) + \frac{1}{2}(z^- - z^+)\nabla \cdot (\boldsymbol{U}_A \mp \frac{1}{2}\boldsymbol{U}) = -\mathcal{D}(-) + \mathcal{S}. \tag{6}$$

If the further simplifying assumption of linearity and a slowly varying background is made, Equation (6) can be solved in the WKB approximation to retain an analytically tractable solution. In the presence of a nonuniform but stationary flow,

the wave action flux $S = \frac{1}{2}\rho|z^+|^2/\omega$, namely the wave energy flux per unit frequency ω, is conserved (see, e.g., Velli 1993, and references therein). Assuming an outwardly directed magnetic field, the wave action conservation in the stationary WKB limit translates into

$$\nabla \cdot (\boldsymbol{U} + \boldsymbol{U}_A)S = 0. \quad (7)$$

Considering that the wave frequency in the absolute (stationary) frame, that is the wave eigenfrequency ω_0, is an invariant, the frequency in the plasma frame ω is given by

$$\omega = \frac{U_A}{U + U_A}\omega_0. \quad (8)$$

Bearing furthermore in mind the mass flux conservation $\rho U r^2 = \text{const}$ and the divergence formula in spherical coordinates for a purely radial vector $\nabla \cdot \boldsymbol{F} = \frac{1}{r^2}\frac{\partial}{\partial r}(r^2 F_r)$, Equation (7) simplifies to

$$\frac{(U + U_A)^2}{UU_A}|z^+|^2 = C, \quad (9)$$

with C being a constant. Equation (9) represents, in the WKB limit, a very useful expression for the radial dependence of the Alfvén wave energy, once estimated at a reference point $r = r_0$ (i.e., at PSP). It predicts that the outwardly propagating Alfvén mode energy peaks (and, therefore, that the turbulence is maximum) where $U = U_A$, i.e., at the Alfvén point. In the case of pure Alfvén waves (i.e., $\sigma_c = \pm 1$ and $\sigma_r = 0$, where σ_c and σ_r are the normalized cross-helicity and residual energy, which measure the imbalances between outward and inward modes and between kinetic and magnetic energies, respectively, e.g., Tu & Marsch 1995), the above equation can also be used for the energy of the magnetic fluctuations E_b. Associating, to a first approximation, the wavelength of turbulence with the expansion of the flow tube, i.e., $\lambda_b \propto \sqrt{A} \sim r$, a complete set of functional forms for estimating the energy transfer rate at the coronal heights observed with Metis is provided.

In the PSP 0.5 hr interval considered in the present analysis (Figure 1(c)), $\sigma_c = 0.97$ and $\sigma_r = -0.10$, suggesting the overwhelming presence of Alfvén waves in the downwind direction. Furthermore, the power spectrum of the magnetic field fluctuations may be compatible with the 5/3 Kolmogorov turbulence (the power-law fit performed at fluid scales to E_b in fact returns a spectral index of 1.61 ± 0.04). It follows that Equation (5) can be safely back-projected from the PSP location, which is below the Alfvén point ($U < U_A$; see Figure 1(c)), into the Metis FOV and thus the coronal heating rate directly derived in the solar corona.

3. Empirical Slow Solar Wind and WKB-like Turbulence Model

Figure 2 shows the solar wind (left panels) and turbulence (right panels) models empirically derived according to the methodological approach described in the previous section (PSP measurements-based estimates are indicated by blue dots). Specifically, Figures 2(a)–(d) display the modeled coronal plasma flow speed, mass density and energy flux, and coronal magnetic field, respectively, compared with the corresponding quantities obtained from the PSI 3D MHD simulations (red lines). In Figure 2(a), also depicted are the Alfvén speed (thin lines) and, for comparison, the spherically symmetric expansion of an isothermal $T = 1.5 \times 10^6$ K-corona (Parker 1958; green line).

Immediately evident is the good agreement, both in radial trends and absolute values, between the empirical model and the outcome of the MHD simulations. This allows a first, prompt consideration. In fact, the two models, in addition to being independently derived, are also the result of somewhat opposite approaches. The MHD simulation is based on a forward modeling driven by (remote) photospheric measurements and the dissipation of Alfvénic turbulence as the mechanism for heating the coronal plasma. The empirical model obtained in this work, on the other hand, is a backward extrapolation based on PSP in situ measurements and the solution of the Euler equations in the WKB limit. Thus, the good agreement between the two models (for both fluid and magnetic parameters) indicates, on the one hand, the accuracy of the present analysis and especially of the Metis observations and, on the other hand, that the aforementioned assumed physical mechanism underlying the heating and subsequent acceleration of the coronal wind complies with observations, again identifying it as the most likely mechanism of coronal heating (in contrast to the alternative high-frequency resonant dissipative processes). More quantitatively, the empirically derived and simulation-based models differ (on average) by 16% for the flow speed, 12% for the plasma density and magnetic field, and 37% for the wind energy flux (for which, as a derived quantity, the discrepancies associated with the fundamental parameters U and ρ obviously widen). In discussing in greater detail the expansion rate of the wind, Figure 2(a) clearly shows that although at the distances observed with Metis the coronal plasma is already largely accelerated, some residual acceleration still persists: in fact, the wind speed increases from ~250 to ~310 km s^{-1} over a range of 7 $R_\odot$. Nevertheless, as evidenced by the basically good agreement with Parker's model, this acceleration may just be thermally driven, which indicates that collisionless field–particle interaction mechanisms for heating (and thereby boosting) the wind are most effective lower than the distances observed with Metis (as, for instance, shown in Telloni et al. 2023). Rough estimates of the power-law radial dependences of the physical quantities displayed in Figures 2(a)–(d), which follow from the continuity equations above and the experimental finding that $\rho \sim r^{-2.21}$, can be given. It turns out that $U \sim r^{0.23}$, $F_w \sim r^{-1.52}$, and $B \sim r^{-1.98}$ for $6.3\ R_\odot < r < 13.3\ R_\odot$.

Figures 2(e)–(g) show the empirically modeled turbulence energy, correlation length, and cascade rate, respectively. As a consequence of Equation (9) and having assumed that $\lambda_b \propto \sqrt{A}$, the fluctuating magnetic energy and the corresponding correlation length decrease from the PSP position toward the Sun (according to $E_b \sim r^{0.45}$ and $\lambda_b \sim r^{0.99}$, respectively). The resulting heating rate in the slow coronal plasma jointly observed with SO/Metis–PSP keeps a relatively constant value throughout the considered heliocentric distances ($\epsilon \sim r^{-0.18}$), in agreement with earlier studies of wind equations and turbulence models (e.g., Dmitruk et al. 2002), which show that the energy per unit mass does not fall off rapidly with altitude. In this regard, it is worth noting that the slight peak in ϵ observed at about 7–8 $R_\odot$ is merely due to the combination of the E_b and λ_b radial trends and, hence, does not indicate any particular underlying physical process. In fact, the heating rate is expected to peak much closer in, at the temperature maximum and the sonic point (around around 2–4 $R_\odot$), i.e.,

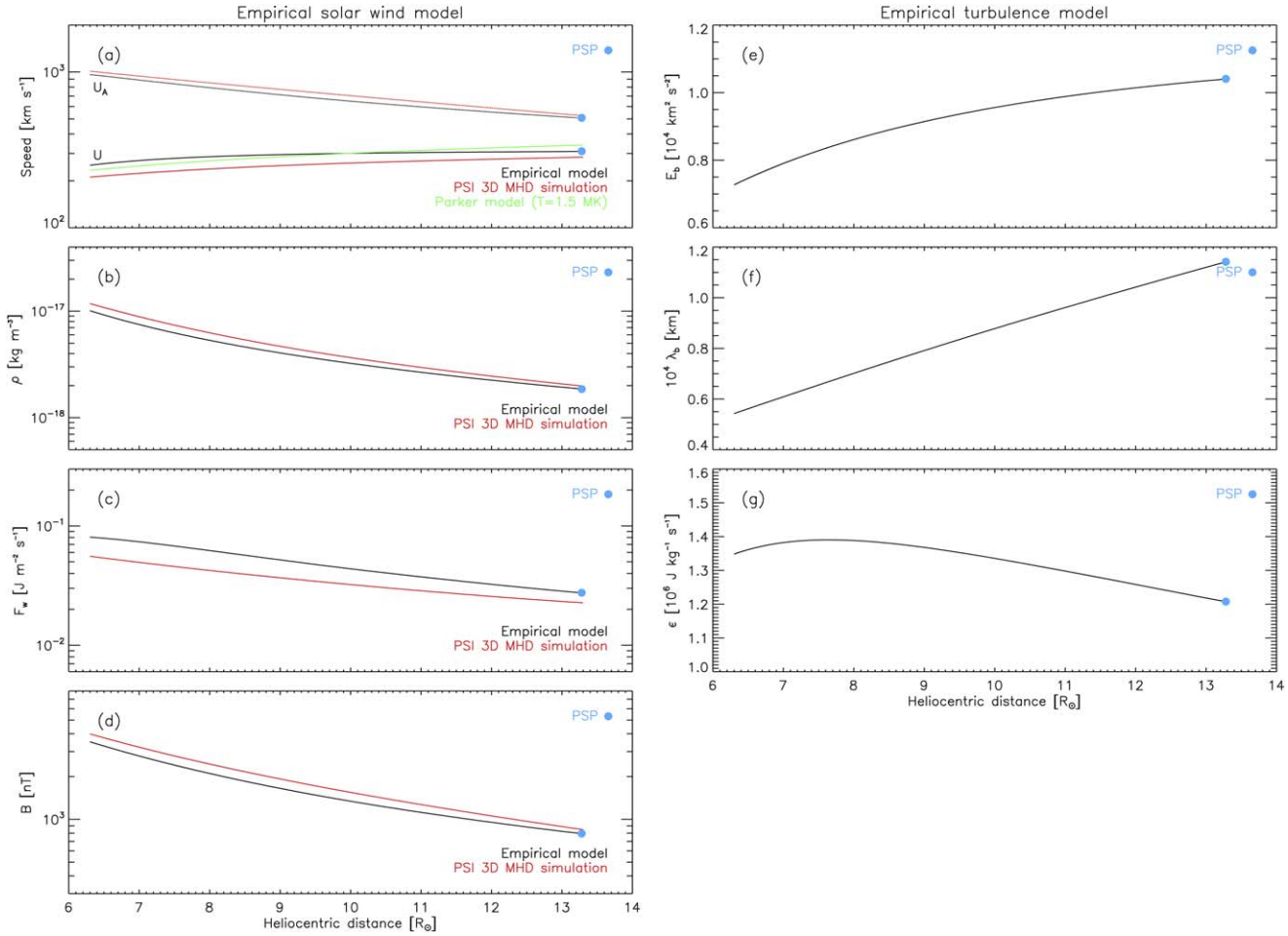

Figure 2. Data-based (black) and physics-based (red) modeling of the radial evolution of the solar wind U (thick lines) and Alfvén U_A (thin lines) speed (a), plasma mass density ρ (b), solar wind flux energy F_w (c), magnetic field B (d), turbulent energy E_b (e) and correlation length λ_b (f), and heating rate ϵ (g) in the slow coronal flow, jointly observed with SO/Metis and PSP during their quadrature on 2022 June 1. The blue dot in each panel refers to the values obtained with PSP measurements. The Parker classical model for an expanding isothermal 1.5 MK corona is shown as a green line in (a).

where plasma heating and acceleration are most effective. The average (turbulent) heating rate per unit volume $\overline{\epsilon\rho} = 5.5 \times 10^{-12}$ J m^{-3} s^{-1} is somewhat lower that the estimates of 10^{-9}–10^{-11} J m^{-3} s^{-1} recently reported by Chandran et al. (2009) and Sasikumar Raja et al. (2021) in approximately the same altitude region (5–45 $R_\odot$). This is not surprising, since these authors provided upper limits for ϵ, whereas those presented here are lower estimates. In fact, the WKB approximation does not take into account the undoubted dissipation of z^+ modes. As a result, the rate at which their energy increases with distance has to be lower than the WKB prediction. Hence, from the PSP position down into the solar corona, this means that their energy E_b would fall off less rapidly, resulting in an energy transfer rate higher than estimated here in the WKB limit. Moreover, under the likely scenario that deeper into the corona the spectrum of the magnetic field fluctuations more closely resembles the turbulence à la Iroshnikov–Kraichnan, for the above, the energy transfer rate would be larger by a factor of $\lambda_b^{-1/4}$, resulting in an average rate per unit volume of 5.2×10^{-11} J m^{-3} s^{-1}, thus at the lower bound of the range of values previously reported in the literature.

The coronal energy loss H, expressed as a flux, can be estimated by integrating the heating rate in the Metis FOV, i.e., from 6.3 to 13.3 $R_\odot$,

$$H = \int \epsilon(r)\rho(r)dr = 2.7 \times 10^{-2}\ \mathrm{J\ m^{-2}\ s^{-1}}. \quad (10)$$

It turns out that H is 33% of the total energy flux of the solar wind ($F_w = 8.1 \times 10^{-2}$ J m^{-2} s^{-1}). This is expected, since, as mentioned just above, most of the acceleration has already taken place at the heights observed with Metis. This energy deposition feeds the observed residual acceleration of the slow solar wind and heats the nonadiabatic coronal plasma. Indeed, in a collisionless plasma with no additional heating, based on the conservation of the Chew–Goldberger–Low (Chew et al. 1956) invariants, the total temperature should scale as $r^{-4/3}$ with distance. This is not observed either in the corona or in interplanetary space (where a radial scaling greater than that predicted by the adiabatic theory of plasma thermal dynamics is found; e.g., Zhao et al. 2019), implying that plasma heating (via turbulence dissipation) occurs, although less significantly, even at distances far beyond where the heating and acceleration processes are most at work (around the sonic point). It is well known that the deficit in internal energy implied by an adiabatic expansion persists at least to 1 au, and in fact well beyond (Richardson et al. 1995; Matthaeus et al. 1999b).

As a final remark, although the present WKB-like analysis is important, as it provides a model-independent and empirical

lower limit of the coronal heating rate (thanks to the coordinated Metis/SO–PSP observations), it should be recalled that it is well known that the radial evolution of the turbulent solar wind can resemble WKB theory even when driven by waves (Roberts 1989) or when turbulent dissipation and shear driving is included (Zank et al. 1996). It is also worth noting that the WKB approximation does not hold in the expanding solar corona. In fact, the wave-only WKB theory predicts no dissipation, whereas turbulence has largely been dissipated far below to accelerate the wind to supersonic speeds. It is therefore evident that a more realistic description of the turbulence evolution from the subsonic wind to the PSP location is needed to compare directly with the Metis observations and thus accurately estimate the (turbulent) heating rate in the solar corona. A variety of turbulence models (e.g., Verdini et al. 2010; Oughton et al. 2011) may be useful as extensions of the present simplified WKB-like model in order to explain observations when linked self-consistently with large-scale MHD equations.

Acknowledgments

Solar Orbiter is a space mission of international collaboration between ESA and NASA, operated by ESA. D.T. was partially supported by the Italian Space Agency (ASI) under contract 2018-30-HH.0. G.P.Z., L.A., and L.-L.Z. acknowledge the partial support of a NASA Parker Solar Probe contract SV4-84017, an NSF EPSCoR RII-Track-1 Cooperative Agreement OIA-2148653, and a NASA IMAP grant through SUB000313/80GSFC19C0027. S.B. and J.K. acknowledge support from NASA contract NNN06AA01C. The Metis program is supported by ASI under contracts to the National Institute for Astrophysics and industrial partners. Metis was built with hardware contributions from Germany (Bundesministerium für Wirtschaft und Energie through the Deutsches Zentrum für Luft- und Raumfahrt e.V.), the Czech Republic (PRODEX), and ESA. The Metis team thanks the former PI, Ester Antonucci, for leading the development of Metis until the final delivery to ESA. D.T. also wishes to thank her for the helpful comments on the paper. The Metis data analyzed in this paper are available from the PI on request. Parker Solar Probe data were downloaded from NASA's Space Physics Data Facility (https://spdf.gsfc.nasa.gov).

ORCID iDs

Daniele Telloni https://orcid.org/0000-0002-6710-8142
Marco Romoli https://orcid.org/0000-0001-9921-1198
Marco Velli https://orcid.org/0000-0002-2381-3106
Gary P. Zank https://orcid.org/0000-0002-4642-6192
Laxman Adhikari https://orcid.org/0000-0003-1549-5256
Cooper Downs https://orcid.org/0000-0003-1759-4354
Aleksandr Burtovoi https://orcid.org/0000-0002-8734-808X
Roberto Susino https://orcid.org/0000-0002-1017-7163
Daniele Spadaro https://orcid.org/0000-0003-3517-8688
Lingling Zhao https://orcid.org/0000-0002-4299-0490
Alessandro Liberatore https://orcid.org/0000-0002-0016-7594
Chen Shi https://orcid.org/0000-0002-2582-7085
Yara De Leo https://orcid.org/0000-0003-2426-2112
Lucia Abbo https://orcid.org/0000-0001-8235-2242
Federica Frassati https://orcid.org/0000-0001-9014-614X
Giovanna Jerse https://orcid.org/0000-0002-0764-7929
Federico Landini https://orcid.org/0000-0001-8244-9749
Gianalfredo Nicolini https://orcid.org/0000-0002-9459-3841
Maurizio Pancrazzi https://orcid.org/0000-0002-3789-2482
Giuliana Russano https://orcid.org/0000-0002-2433-8706
Clementina Sasso https://orcid.org/0000-0002-5163-5837
Vincenzo Andretta https://orcid.org/0000-0003-1962-9741
Vania Da Deppo https://orcid.org/0000-0001-6273-8738
Silvano Fineschi https://orcid.org/0000-0002-2789-816X
Catia Grimani https://orcid.org/0000-0002-5467-6386
Petr Heinzel https://orcid.org/0000-0002-5778-2600
John D. Moses https://orcid.org/0000-0001-9670-2063
Giampiero Naletto https://orcid.org/0000-0003-2007-3138
Marco Stangalini https://orcid.org/0000-0002-5365-7546
Luca Teriaca https://orcid.org/0000-0001-7298-2320
Michela Uslenghi https://orcid.org/0000-0002-7585-8605
Arkadiusz Berlicki https://orcid.org/0000-0002-6505-4478
Roberto Bruno https://orcid.org/0000-0002-2152-0115
Gerardo Capobianco https://orcid.org/0000-0003-0520-2528
Giuseppe E. Capuano https://orcid.org/0000-0002-8430-8218
Chiara Casini https://orcid.org/0000-0001-8783-0047
Marta Casti https://orcid.org/0000-0002-9716-3820
Paolo Chioetto https://orcid.org/0000-0002-3379-2142
Alain J. Corso https://orcid.org/0000-0003-0378-9249
Raffaella D'Amicis https://orcid.org/0000-0003-2647-117X
Michele Fabi https://orcid.org/0000-0002-2464-1369
Fabio Frassetto https://orcid.org/0000-0001-5528-1995
Marina Giarrusso https://orcid.org/0000-0002-4453-1597
Silvio Giordano https://orcid.org/0000-0002-3468-8566
Salvo L. Guglielmino https://orcid.org/0000-0002-1837-2262
Enrico Magli https://orcid.org/0000-0002-0901-0251
Giuseppe Massone https://orcid.org/0000-0002-2656-1557
Mauro Messerotti https://orcid.org/0000-0002-5422-1963
Giuseppe Nisticò https://orcid.org/0000-0003-2566-2820
Maria G. Pelizzo https://orcid.org/0000-0002-1383-6750
Fabio Reale https://orcid.org/0000-0002-1820-4824
Paolo Romano https://orcid.org/0000-0001-7066-6674
Udo Schühle https://orcid.org/0000-0001-6060-9078
Sami K. Solanki https://orcid.org/0000-0002-3418-8449
Thomas Straus https://orcid.org/0000-0002-6280-806X
Rita Ventura https://orcid.org/0000-0002-5152-0482
Cosimo A. Volpicelli https://orcid.org/0000-0002-4997-1460
Luca Zangrilli https://orcid.org/0000-0002-4184-2031
Gaetano Zimbardo https://orcid.org/0000-0002-9207-2647
Paola Zuppella https://orcid.org/0000-0003-0290-3193
Stuart D. Bale https://orcid.org/0000-0002-1989-3596
Justin C. Kasper https://orcid.org/0000-0002-7077-930X

References

Adhikari, L., Zank, G. P., Telloni, D., et al. 2017, ApJ, 851, 117
Adhikari, L., Zank, G. P., Zhao, L. L., & Telloni, D. 2022, ApJ, 938, 120
Andrés, N., Sahraoui, F., Galtier, S., et al. 2019, PhRvL, 123, 245101
Antonucci, E., Downs, C., Capuano, G. E., et al. 2023, PhPl, 30, 022905
Antonucci, E., Romoli, M., Andretta, V., et al. 2020, A&A, 642, A10
Chandran, B. D. G., Quataert, E., Howes, G. G., Xia, Q., & Pongkitiwanichakul, P. 2009, ApJ, 707, 1668
Chen, C. H. K., Bale, S. D., Bonnell, J. W., et al. 2020, ApJS, 246, 53

Chew, G. F., Goldberger, M. L., & Low, F. E. 1956, RSPSA, 236, 112
Cranmer, S. R. 2020, ApJ, 900, 105
De Leo, Y., Burtovoi, A., Teriaca, L., et al. 2023, A&A, in press
Dmitruk, P., Matthaeus, W. H., Milano, L. J., et al. 2002, ApJ, 575, 571
Duan, D., Bowen, T. A., Chen, C. H. K., et al. 2020, ApJS, 246, 55
Fineschi, S., Naletto, G., Romoli, M., et al. 2020, ExA, 49, 239
Fox, N. J., Velli, M. C., Bale, S. D., et al. 2016, SSRv, 204, 7
Hayes, A. P., Vourlidas, A., & Howard, R. A. 2001, ApJ, 548, 1081
Holzer, T. E., & Axford, W. I. 1970, ARA&A, 8, 31
Howard, R. A., Vourlidas, A., Bothmer, V., et al. 2019, Natur, 576, 232
Iroshnikov, P. S. 1963, AZh, 40, 742
Kolmogorov, A. 1941, DoSSR, 30, 301
Kraichnan, R. H. 1965, PhFl, 8, 1385
Marino, R., & Sorriso-Valvo, L. 2023, PhR, 1006, 1
Matthaeus, W. H., Zank, G. P., Oughton, S., Mullan, D. J., & Dmitruk, P. 1999a, ApJL, 523, L93
Matthaeus, W. H., Zank, G. P., Smith, C. W., & Oughton, S. 1999b, PhRvL, 82, 3444
McKenzie, J. F., Banaszkiewicz, M., & Axford, W. I. 1995, A&A, 303, L45
Mikić, Z., Downs, C., Linker, J. A., et al. 2018, NatAs, 2, 913
Moses, J. D., Antonucci, E., Newmark, J., et al. 2020, NatAs, 4, 1134
Müller, D., Cyr, O. C., St., Zouganelis, I., et al. 2020, A&A, 642, A1
Oughton, S., Matthaeus, W. H., Smith, C. W., Breech, B., & Isenberg, P. A. 2011, JGRA, 116, A08105
Parker, E. N. 1958, ApJ, 128, 664
Pesnell, W. D., Thompson, B. J., & Chamberlin, P. C. 2012, SoPh, 275, 3
Politano, H., & Pouquet, A. 1998, GeoRL, 25, 273
Richardson, J. D., Paularena, K. I., Lazarus, A. J., & Belcher, J. W. 1995, GeoRL, 22, 325
Roberts, D. A. 1989, JGR, 94, 6899
Romoli, M., Antonucci, E., Andretta, V., et al. 2021, A&A, 656, A32
Sasikumar Raja, K., Subramanian, P., Ingale, M., Ramesh, R., & Maksimovic, M. 2021, ApJ, 914, 137
Scherrer, P. H., Schou, J., Bush, R. I., et al. 2012, SoPh, 275, 207
Sorriso-Valvo, L., Marino, R., Carbone, V., et al. 2007, PhRvL, 99, 115001
Telloni, D., Adhikari, L., Zank, G. P., et al. 2022b, ApJL, 938, L8
Telloni, D., Andretta, V., Antonucci, E., et al. 2021a, ApJL, 920, L14
Telloni, D., Antonucci, E., Adhikari, L., et al. 2023, A&A, 670, L18
Telloni, D., Sorriso-Valvo, L., Woodham, L. D., et al. 2021b, ApJL, 912, L21
Telloni, D., Zank, G. P., Sorriso-Valvo, L., et al. 2022a, ApJ, 935, 112
Titov, V. S., Mikić, Z., Linker, J. A., Lionello, R., & Antiochos, S. K. 2011, ApJ, 731, 111
Tu, C.-Y. 1988, JGR, 93, 7
Tu, C. Y., & Marsch, E. 1995, SSRv, 73, 1
Usmanov, A. V., Goldstein, M. L., & Matthaeus, W. H. 2014, ApJ, 788, 43
van de Hulst, H. C. 1950, BAN, 11, 135
Velli, M. 1993, A&A, 270, 304
Verdini, A., Velli, M., Matthaeus, W. H., Oughton, S., & Dmitruk, P. 2010, ApJL, 708, L116
Wang, B. B., Zank, G. P., Adhikari, L., & Zhao, L. L. 2022, ApJ, 928, 176
Wang, Y. M. 1994, ApJL, 437, L67
Wenzel, K. P., Marsden, R. G., Page, D. E., & Smith, E. J. 1992, A&AS, 92, 207
Wu, H., Tu, C., Wang, X., He, J., & Yang, L. 2020, ApJL, 904, L8
Zank, G. P., Matthaeus, W. H., & Smith, C. W. 1996, JGR, 101, 17093
Zhao, L. L., Zank, G. P., & Adhikari, L. 2019, ApJ, 879, 32
Zhao, L. L., Zank, G. P., Telloni, D., et al. 2022, ApJL, 928, L15
Zhou, Y., & Matthaeus, W. H. 1990, JGR, 95, 10291